Journal of Cleaner Production 238 (2019) 117881

Contents lists available at ScienceDirect

Journal of Cleaner Production

journal homepage: www.elsevier.com/locate/jclepro

Spatio-temporal patterns of traffic-related air pollutant emissions in different urban functional zones estimated by real-time video and deep learning technique

Jinchao Song [a, b], Chunli Zhao [c, d], Tao Lin [a, **], Xinhu Li [a, e, *], Alexander V. Prishchepov [b]

[a] Key Lab of Urban Environment and Health, Institute of Urban Environment, Chinese Academy of Sciences, Xiamen, 361021, China
[b] Department of Geosciences and Natural Resource Management (IGN), University of Copenhagen, Øster Voldgade 10, 1350, Copenhagen, Denmark
[c] Faculty of Engineering, LTH, Department of Technology and Society, Transport & Roads, Lund University, 22100, Lund, Sweden
[d] K2 – the Swedish Knowledge Centre for Public Transport, Lund, Sweden
[e] College of Architecture and Urban Planning, Tongji University, Shanghai, 200082, China

ARTICLE INFO

Article history:
Received 30 November 2018
Received in revised form
6 July 2019
Accepted 1 August 2019
Available online 8 August 2019

Handling Editor: Zheming Tong

Keywords:
Pollutant emissions
Urban functional zones
Video-based vehicle detection
Deep learning

ABSTRACT

The aim of this paper is to explore the relationship between spatial-temporal patterns of vehicles types and numbers in different urban functional zones and traffic-related air pollutant emissions with real-time traffic data collected from traffic surveillance video and image recognition. The data were analyzed by using video-based detection technique, while the air pollution was quantified via pollutant emission coefficients. The results revealed that: (1) the order of traffic-related pollutant emissions was expressway > business zone > industrial zone > residential zone > port; (2) daily maximum emissions of each pollutant occurred in different functional zones on weekdays and weekends. With the exception of expressway, the business zones had the highest emissions of CO, HC and VOC on weekdays, while the highest emissions of all the pollutants (CO, HC, NOx, PM2.5, PM1.0, and VOC) were at the weekend. The industrial zone had the highest emissions of NOx, PM2.5 and PM1.0 on weekdays; (3) pollutant emissions (CO, HC, NOx, PM2.5, PM1.0 and VOC) in all functional zones peaked in the morning and evening peak except at port sites; (4) cars and motorcycles represented the major source of traffic-related pollutant emissions. Collecting data through video-based vehicle detection with finer spatio-temporal resolution represents a cost-effective way of mapping spatio-temporal patterns of traffic-related air pollution to contribute to urban planning and climate change studies.

1. Introduction

Exposure to air pollution adversely affects human health (Brugge et al., 2007; Künzli et al., 2000; Lelieveld et al., 2015). Despite significant improvements in fuel and engine technology, today's urban atmospheric environment is primarily polluted by traffic emissions (Colvile et al., 2001), which represents a serious hazard to human health (Hoek et al., 2011). The main traffic-related pollutants are carbonic oxide (CO), hydrocarbons (HC), volatile organic compounds (VOC), Nitrogen Oxides (NOx) and particles (Vardoulakis et al., 2003). Outdoor air pollution, particularly PM2.5, results in 3.3 million premature deaths annually worldwide, predominantly in Asia (Lelieveld et al., 2015). According to previous research, atmospheric pollutants are responsible for various acute and chronic conditions in humans. For instance, CO is an asphyxiating pollutant that reduces the ability of blood to carry oxygen to the organs (Lelieveld et al., 2015). Furthermore, nitrogen oxides increase susceptibility to respiratory infections (Kampa et al., 2008), while particulate matter results in lung inflammation and blood irritation (Riediker et al., 2001). In urban environments, particularly in areas with relatively high population and traffic density, exposure to hazardous substances is significantly increased, and atmospheric pollutants are regulated with respect to different exposure durations (Vardoulakis et al., 2003).

Urban functional zones (e.g., residential zones, industrial zones), which are parcels divided by the road network, have become the

* Corresponding author. Key Lab of Urban Environment and Health, Institute of Urban Environment, Chinese Academy of Sciences, Xiamen, 361021, China.
** Corresponding author.
E-mail addresses: jiso@ign.ku.dk (J. Song), tlin@iue.ac.cn (T. Lin), xhli@tongji.edu.cn (X. Li).

https://doi.org/10.1016/j.jclepro.2019.117881
0959-6526/

basic units of quantitative analysis in refined urban planning and management and provide detail about urban built environments (Song et al., 2018; Song et al., 2019a; Song et al., 2019b). Previous studies have found that functional zones have obvious impacts on travel behavior and transportation (Zhao et al., 2018a, b; Vardoulakis et al., 2003) and that pollutant emissions vary according to vehicle types (Hassani et al., 2016; Na et al., 2015). Traffic-related air pollution near roads can vary significantly both spatially and temporally (Karner et al., 2010; Kimbrough et al., 2013), and individuals, especially children, who live or work near truck routes and highways are particularly susceptible to asthma and other diseases (Brauer et al., 2002; Gordian et al., 2006). This finding is also supported by the data from air pollution monitoring stations, which indicate that individuals who live next to main roads have much higher relative risks of death than those who do not live close to such roads (Kim et al., 2015). Travel activities and travel modes are closely related to functional zones/land use (Cao et al., 2017; Ewing et al., 2010; Kockelman, 1997). Pollutant emissions display significant spatial variability across different urban functional zones, land use patterns and the distribution of traffic often lead to inequities in terms of exposure to vehicle-related air pollutants (Roemer et al., 2018). Land-use regression models have been used to model traffic-related air pollution (Buzzelli et al., 2011; Dons et al., 2013a, b; Henderson, 2007; Jerrett, 2009; Levy et al., 2015; Rosenlund et al., 2008; Shekarrizfard et al., 2016; Wang et al., 2013). The spatial characterization of vehicle types and pollutant emissions is complicated by street canyons and roadside structures in urban areas (Dons et al., 2013a, b; Duvall et al., 2012; Jerrett et al., 2005). For instance, local traffic and elemental carbon exhibit significantly more variability and complex relationships for NO2 than for PM2.5 in European cities (Clougherty et al., 2008). The strong association between traffic density and annual averages of NO2 concentration and PM2.5 absorbance are considered as a proxy for soot (Hochadel et al., 2006). For these reasons, estimating traffic-related air pollution based on road function requires an understanding of spatial distribution and temporal changes in vehicles and amounts. However, the spatio-temporal resolution of such research is coarse as it is very labor-intensive and requires expensive instruments. Therefore, previous studies have rarely provided sufficient data for high-resolution spatial and temporal analysis of pollutant emissions.

Furthermore, due to data and algorithm limitations, few researchers have quantified the relationship between functional zones and the spatio-temporal distribution of traffic-related air pollution at finer spatio-temporal resolution. Commonly, air pollution models that adopt the spatial interpolation method use data from air quality monitoring stations (Hoogh et al., 2018; Wu et al., 2018). However, these approaches, which are based on models with coarse spatio-temporal resolution at a large scale, have ignored the influence of pollutant diffusion in relation to, e.g. terrain, building height and density. Fortunately, surveillance video and image cognition algorithms can improve the accuracy and efficiency of vehicle detection and vehicle counts (Al-smadi, 2016). Deep-learning techniques have performed impressively in terms of detecting objects (Esteva et al., 2017; Xu et al., 2017). A number of methods have subsequently been proposed based on such techniques including the region-based convolutional neural network (R—CNN) (Girshick, 2015), Fast-R-CNN, the single shot multi-box detector (Leibe et al., 2016) and “You only look once” (YOLO) (Redmon et al., 2016.). YOLO is a state-of-the-art real-time framework for the detection by jointly optimizing detection and classification. Furthermore, YOLO can achieve real-time performance on a powerful GPU (Al-smadi, 2016). Hence, this study has utilized YOLO to categorize and count vehicles.

The aim of this study is to quantify the spatial-temporal patterns of traffic-related pollutant emissions and to observe the relationship between air pollutants and the vehicles’ spatial distribution on the roads in different urban functional zones. The intention is to provide fundamental cross-sectional knowledge to help reduce traffic-related air pollutant emissions and, thereby, improve air quality. This study has the following three objectives: (1) detect and count vehicles through the use of a novel approach (YOLO) by using real-time traffic video; (2) map six traffic-related pollutants ($PM_{2.5}$, PM1.0, CO, HC, VOC, and NOx) across different time and urban functional zones; (3) observe the relationship between urban functional zones and spatio-temporal patterns of traffic-related air pollutants.

2. Materials

2.1. Study area and sampling sites

The Haicang district in the west of Xiamen City in southeastern China (Fig. 1) was selected as the study site. According to land use status published by the local Haicang government (XMHOUSE, 2016), the district includes the following five urban functional zones: residential, industrial, business, port and non-built area (Fig. 1). The Haicang district is a mixed urban and industrial zone located on the coast with a total area of 173.6 km^2 and a population of 140,000. The district attracts significant investment from Taiwanese business developers. Many factories are located in the southeast of Haicang with an area of 10.7 km^2. The northern industrial zone in Haicang includes more than 40 factories for refining chemicals and producing plastic, rubber and construction material with an area of 20.6 km^2. The residential area and the adjacent undeveloped area around the industrial zone is a major suburb. The area in the south of Haicang includes a harbor and warehouses and is characterized by port, energy-related industry with a total area of 12.4 km^2.

Haicang district is an industry-oriented zone, which means it

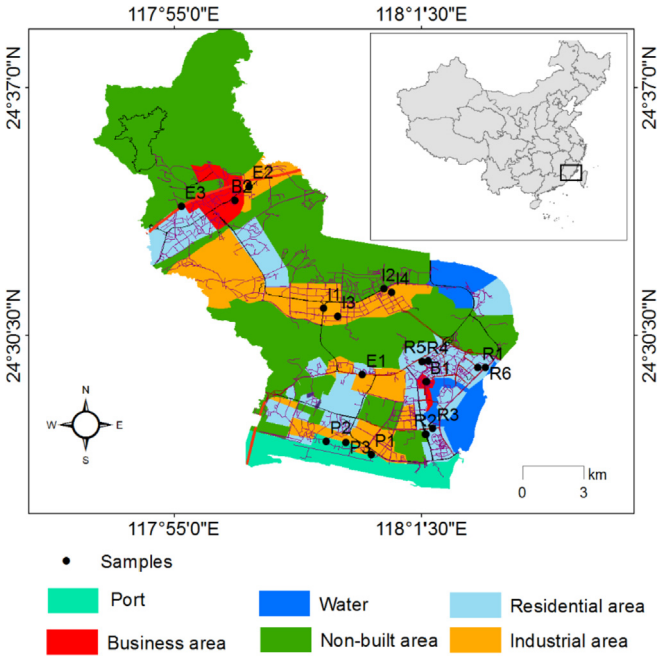

Fig. 1. Eighteen sampling sites located on expressways and branch roads in different urban functional zones in the Haicang district. R_n represents the residential area; E_n represents the expressway; P_n represents the port; I_n represents the industrial area; Bn represents the business zone.

has many factories and a greater number of heavy goods vehicles. In order to collect comprehensive information on the various types and models of vehicles passing through the functional zones, it is necessary to select suitable sampling points where the majority of the vehicles will be recorded by camera. Therefore, the study set up sampling sites on the expressways and urban roads in the different functional zones. According to road classification and road function, branch roads are intra-regional and serve vehicles coming from nearby functional zones, while highways are inter-functional roads that connect neighboring cities to Xiamen (Song et al., 2019a). According to the urban functional zone map, the total residential, business, industrial and port area is 29.8 km^2, 6.1 km^2, 31 km^2, and 12.4 km^2, respectively. Population density and road density are lower in the industrial zone than in the residential and business zones. Therefore, according to the proportion of functional zone area and the stratified sampling rule, we sampled 18 points in line with the area of each functional zone (Fig. 1). At the sampling sites, traffic information is continuously recorded by the video 24/7 from Monday to Sunday. The name and location of the sites are as follows (see Fig. 1): three sites on the expressway - E1, E2, and E3; six sites in the residential area - R1, R2, R3, R4, R5 and R6; three sites in the port area - P1, P2 and P3; four sites in the industrial area - I1, I2, I3 and I4, and two sites in the business area - B1, B2. According to the Statistical Yearbook (2017) (http://www.stats-xm.gov.cn/2017/), there were 1.4 million vehicles 46% of which were private cars, 11% trucks and 33% motorcycles.

2.2. Data source and pre-processing

To quantify traffic-related air pollution, traffic was recorded (.avi) at the sample sites to document the different types of vehicle and the total number of vehicles, while the total number of each type of vehicle was counted every hour. The frame width, height and frame rate of the video recording was 1440 pixels, 1080 pixels, and 25 frames/second, respectively. The number of vehicles multiplied by the pollutant emissions coefficient of each type of vehicle. The coefficient of pollutant emissions for each vehicle type was taken from Xiamen car ownership statistics (2016) and the Vehicular Emission Inventory in China (Yang et al., 2018; Zhou et al., 2015). The pollutant emissions coefficient for each type of vehicle are presented in Table 1.

3. Data collection and analysis

3.1. Vehicle detection

YOLO was applied to detect the type of vehicles and count the total number of each type of vehicle. It employs a single convolutional network to predict multiple bounding boxes and class probabilities for those boxes. The YOLO network uses features from the entire image to predict each bounding box and predicts all bounding boxes across all classes. The system detects vehicles in the following way (Fig. 2) (Redmon et al., 2016): first, YOLO divided the input image into a 7×7 grid ($S \times S$), and then predicted bounding boxes (B) and confidence scores for those boxes in each grid cell. The confidence level reflects how confident the model is that a box contains an object and how accurate it considers the box that it predicts. Each bounding box contains five predictions: (x, y, w, h) and indicates confidence, where x, y, w, h represent the centre of the box relative to the bounds of the grid cell and the width and height of box. $B = 2$ (number of bounding box in a grid cell) was used according to our image size and view angle. After that, the system predicts C conditional class probabilities in each grid cell, which were conditioned on the grid cells containing an object. In this research, $C = 9$ was applied according to our vehicles categories in line with Redmon et al. (2016). In this study, the result of tension should be: $S \times S \times (B \times 5 + C) = 7 \times 7 \times (2 \times 5 + 9)$.

The system multiplied the class probabilities and confidence at the test time, which yields the specific class confidence scores for each box. Output in each grid cell includes properties of two bounding boxes and classification. In each bounding box, $(b_x\ ,\ b_y\ ,\ b_w\ ,\ b_h\ )$ means the centre point of the bounding box (Fig. 3). For i^{th} class, C_i means confidence of object which exist in the bounding box. 0 represents no object while 1 represents there is object (Formula (1)). $P_i(c_i)$ represents possibility of classification.

$$\begin{aligned} y_{output} &= |Bbox_{1i}|Bbox_{2i}|P_i(c)| \\ &= |C_{i,1}, b_{xi,1}, b_{yi,1}\, b_{wi,1}\, b_{hi,1}|C_{i,2}, b_{xi,2}, b_{yi,2}\, b_{wi,2}\, b_{hi,2}|P_i(c_1), \\ P_i(c_2), P_i(c_3) \ldots P_i(c_{14})| \end{aligned} \tag{1}$$

To optimize the detection, loss function include four parts: the difference of coordinate (x, y) and width (w) and height (h) of bounding box between predicting value and ground truth, the confidence in a bounding box which is with object and without object, and possibility of classification (Formula (2)).

$$\begin{aligned} \text{Loss Function} = {} & \mu_{coord} \sum_{i=0}^{S^2} \sum_{j=0}^{B} I_{ij}^{obj} \left[(x_i - \hat{x}_i)^2 + (y_i - \hat{y}_i)^2 \right] \\ & + \mu_{coord} \sum_{i=0}^{S^2} \sum_{j=0}^{B} I_{ij}^{obj} \left[\left(\sqrt{w_i} - \sqrt{\widehat{w_i}} \right)^2 + \left(\sqrt{h_i} - \sqrt{\widehat{h_i}} \right)^2 \right] \\ & + \sum_{i=0}^{S^2} \sum_{j=0}^{B} I_{ij}^{obj} (c_i - \hat{c}_i)^2 + \mu_{noobject} \sum_{i=0}^{S^2} \sum_{j=0}^{B} I_{ij}^{obj} (c_i - \hat{c}_i)^2 \\ & + \sum_{i=0}^{S^2} I_i^{obj} \sum_{C \in class} \left(P_i(c) - \widehat{P_i(c)} \right)^2 \end{aligned} \tag{2}$$

Finally, a moving vehicle was counted when it passes the baseline. As shown in Fig. 2, when a vehicle passed through the area with the black line (Fig. 2. Final output), the frame was recorded.

Table 1
Pollutant emissions coefficient for each vehicle type.

Vehicle and fuel types		Pollutant emissions (g/km)					
Vehicle	Fuel	CO	HC	NOx	PM2.5	PM1.0	VOC(mg/km)
Car	Gasoline	2.9461	0.3349	0.2443	0.0094	0.0104	0.5094
Medium bus	Gasoline	21.4300	2.5670	1.7810	0.0600	0.0670	0.9616
Large bus	Diesel	8.8902	1.2000	11.1109	0.9600	1.0666	0.4182
Light truck	Gasoline	23.3412	2.4535	1.7123	0.0414	0.0461	1.9538
Medium truck	Diesel	5.4373	1.5570	7.5948	0.7897	0.8750	0.3116
Heavy truck	Diesel	5.4911	1.2688	8.9964	0.5646	0.6225	0.3717
Taxi	Gasoline and others	4.7218	0.5586	0.3443	0.0094	0.0104	0.3816
Public bus	Diesel	9.2864	1.2000	11.1109	0.9481	1.0666	0.7688
Motorcycle	Gasoline	8.1652	1.1327				

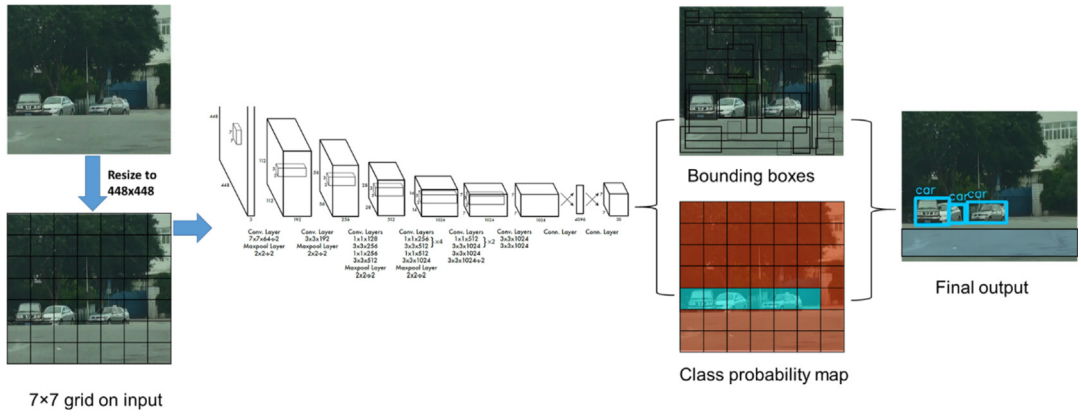

Fig. 2. YOLO detection process (Redmon et al., 2016). The system divides the image into a 7 × 7 grid and then predicts 2 bounding boxes for each grid cell. The line in the final output image was used for counting the vehicles. The network includes 24 convolutional layers and 2 fully connected layers. The line in the final output image was used for counting the vehicles.

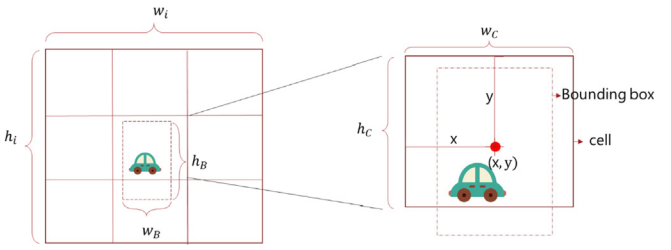

Fig. 3. Defining centre point for bounding box. $b_w = w_B/w_i$, $b_h = h_B/h_i$, $b_x = x/w_C$, $b_y = y/w_C$. Probability of class 1 in a bounding box is calculated by: $P_i(class1) \times IOU_{truth} =$ P (class1|object) × P (object) × IOU_{truth}, $IOU_{truth}^{truth} = \frac{Area_{(Detection\ result)} \cap Area_{(Groundtruth\ result)}}{Area_{(Detection\ result)} \cup Area_{(Groundtruth\ result)}}$, $P_i(c_1) =$ P (class1|object)

Through this process, YOLO learns generalizable representations of objects from the entire image. We then use YOLO as the vehicle detection method in the proposed framework. YOLO could achieve 62.5 mAP using GPU. The accuracy based on dark flow indicates that YOLO achieved the highest accuracy when detecting buses (79.8%), while the lowest accuracy was for trucks (76.5%). Training and testing dataset were cited from Pascal VOC (https://pjreddie.com/projects/pascal-voc-dataset-mirror/) and ImageNet (http://www.image-net.org/).

3.2. Spatio-temporal pattern analysis

The number of vehicles that were counted every hour during weekdays and weekends represents the spatio-temporal pattern of the vehicles in different functional zones. The daily totals of vehicles and the mean value were acquired. Sequentially, the daily spatio-temporal emissions of different pollutants were correspondingly calculated. To explore the relationship between air pollution and spatiotemporal patterns of traffic at the various sampling sites, we mapped and analyzed the trend in pollutant emission patterns in each of the functional zones, which is discussed in the results section below.

4. Results

4.1. Spatio-temporal pattern of vehicle numbers

4.1.1. Total number of vehicles per day

The total number of vehicles was higher during weekdays than weekends in all functional zones. On weekdays, there were more vehicles on the expressway (24,328 vehicles per day) than on other roads, followed by the business area (12,075 vehicles per day) (Fig. 3). On the expressway and roads in the port zone, cars were the most common vehicles (expressway, 14,533; port, 1376), followed by heavy trucks (expressway, 3300; port, 1289). In the other zones, cars were most frequently detected, followed by motorcycles. For instance, of the 12,075 vehicles that were detected in business zone, 8187 were cars and 1734 were motorcycles. Compared with the other zones, the business area had the highest number of cars, medium-sized buses, taxis and public buses, while the industrial area had the highest number of large buses, medium buses, medium trucks and motorcycles. The port area had the highest number of heavy trucks.

Even though the total number of vehicles was higher on weekdays than at weekends, some special cases indicated an opposite situation. In the business area, the number of taxis at the weekend (588) was higher than during the weekdays (245), which was also the case for large buses (142 at weekends vs. 78 on weekdays). A similar pattern of more of one specific type of vehicle being observed at the weekend than during the weekdays was observed in several other cases. For instance, the number of cars and medium-sized buses at E1 and E3, the number of medium-sized buses and large buses at R1 and R6, the number of motorcycles R2, R4 and R5, and the number of large buses at P1, P2, I1 and I2.

4.1.2. Time series change

As shown in Fig. 4, cars and motorcycles account for the largest proportion of total vehicles. Therefore, we take cars and motorcycles as the case study to analyze the time series change on weekdays and weekends.

(1) Car

In the business, industrial and expressway zones, there were more cars during the evening peak than during the morning peak on weekdays. However, at the weekend, no peak hour patterns were observed in the three zones. In the port and residential zones, the number of cars during the morning peak was similar to the number observed during the evening peak on weekdays. In the port area, the number of cars at the weekend (647) was less than half of the total observed on weekdays (1376). In the residential zone, the morning peak of car numbers on weekend occurred 3 h late than weekday.

(2) Motorcycles

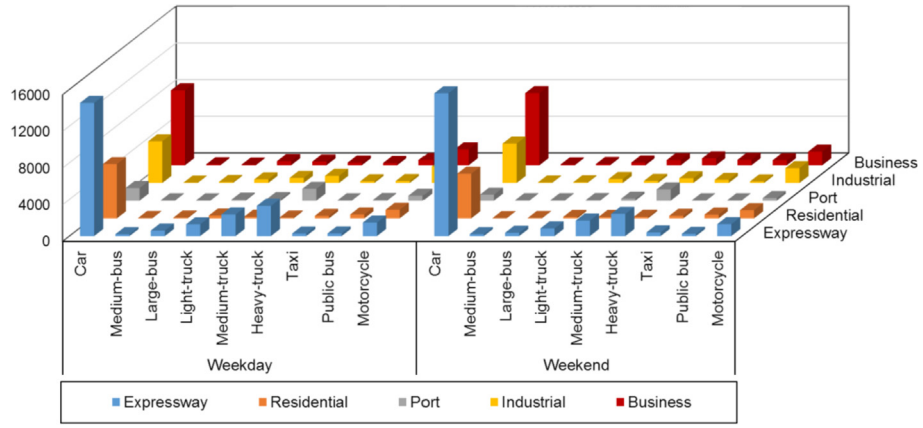

Fig. 4. Daily mean values for number of vehicles on weekdays and weekends in the urban functional zones in Haicang.

With the exception of the expressway, the largest number of motorcycles was detected in the industrial zone, where the number of motorcycles increased after 7 p.m. (I2, I3 and I4). The number of motorcycles in the port area was less than in the other areas. On weekdays, the number of motorcycles peaked in the morning and evening in all functional zones. In the business zones, there was a morning peak (120 per hour) and an evening peak (225 motorcycles per hour) on weekdays. More specifically, the business zones had a peak period around 11am with 120 motorcycles per hour.

At the weekends, there was an obvious evening peak in the residential zone (250 per hour) and expressway (125 per hour), but there was no morning peak. The number of motorcycles in the business zone increased to 125 per hour from 8 a.m., and maintained a high volume during the daytime.

4.2. Spatio-temporal pattern of pollutant emissions

4.2.1. Total pollutant emissions per day

Pollutant emissions were higher on expressways than on other roads (Table 2 and Fig. 6). On weekdays, the business zones showed the highest level of emissions of CO, HC and VOC, while the industrial zones had the highest level of NOx, PM2.5 and PM1.0 emissions. At weekends, all pollutant emissions (CO, HC, NOx, PM2.5, PM1.0 and VOC) in the business zones were higher than in other zones.

Each maximum for the emissions of pollutants occurred in different zones on weekdays and at weekends. For instance, B1 had the highest emissions of CO both on weekdays (75580 g/km) and at weekends (67402 g/km), and the highest emissions of VOC on weekdays (13779 g/km). At the B2 site, all the pollutants were twice as high at weekends than on weekdays. The B2 site had the highest emissions of HC (9020 g/km) and PM2.5 (1638 g/km) on weekdays, and PM1.0 at weekends (2515 g/km). P1 had the highest emissions of NOx (22972 g/km) on weekdays, and I4 had the highest emissions of NOx (29859 g/km) at weekends.

4.2.2. Time series change in pollutant emissions

From the perspective of time series changes (Fig. 6), pollutants (CO, HC, NOx, PM2.5, PM1.0 and VOC) in all functional zones had a morning and evening peak period except at the port sites. The pollutant emissions during the peak period at the expressway sites were triple (CO, NOx) or twice (VOC, HC, PM2.5, PM1.0) as high as those at the residential and industrial sites. All pollutants at the business sites during the peak period were also higher than they were at other sites, while port sites had the lowest values. During the peak period, the change in emissions of CO (4200 g/km), VOC (700 mg/km), NOx (1000 g/km), HC (500 g/km), PM2.5 (100 g/km), and PM1.0 (50 g/km) at the residential and industrial sites were synchronous.

As illustrated in Fig. 7, the highest pollutant emissions occurred in the residential, industrial and business zones. We take the morning peak and evening peak in pollutant emissions in the residential, industrial and business zones as case studies to analyze the main sources of pollutants (Fig. 7). In the R6 residential zone, the average number of motorcycles reached a high of 433 per hour during the morning peak. The highest emissions of VOC occurred at R6 during the morning peak (08:00–09:00). Specifically, emissions of VOC from motorcycles (57.13%) were higher than from cars (37.99%). In the industrial zone, emissions of VOC reached a high of 800 mg/km during the evening peak period on weekdays (I2 and I3). Unlike the R6 site, at the I2 site, the emissions of VOC from motorcycles during the morning peak were 53.91%, while emissions of VOC from light trucks (18.71%) were nearly as high as VOC emissions from cars (24.79%). At B1, during the evening peak period, the emissions (1000 g/km for HC, 1200 mg/km for VOC) were higher than during other periods. Emissions of VOC were higher from cars (46.46%) than from motorcycles (38.77%). Unlike VOC, emissions of HC were higher from cars (41.43%) than from motorcycles (23.81%), whereas medium buses (12.05%) and light trucks (11.51%) were responsible for 23.6% of HC emissions. At these sites, cars and motorcycles are the major sources of pollutant

Table 2
Daily mean values of pollutant emissions across different functional zones on weekdays and at weekends.

	CO(g/km)		HC(g/km)		NOx (g/km)		PM2.5 (g/km)		PM1.0 (g/km)		VOC(mg/km)	
	Weekday	Weekend	Weekday	Weekend	Weekday	Weekend	Weekday	Weekend	Weekday	Weekend	Weekday	Weekend
Highway	127794	110509	19067	15954	61617	47276	4754	3628	5110	3882	16269	14960
Residence	40343	34720	5016	4403	9978	9385	844	789	845	785	6552	5729
Port	19586	13944	3320	2643	14142	13476	977	950	1023	1016	1706	2837
Industrial	49243	43896	6975	5825	16711	10726	1434	907	1402	838	8410	7616
Business	60798	63944	7836	8612	14458	21882	1255	1794	1218	1841	10198	9904

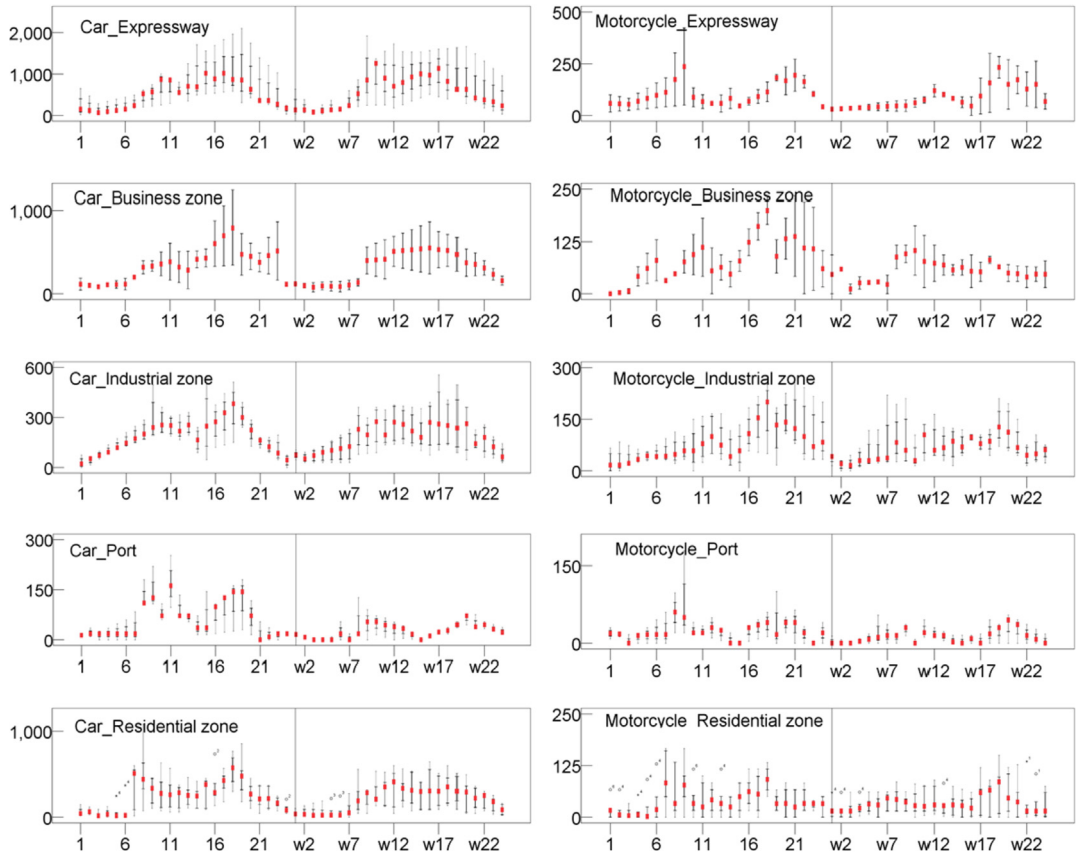

Fig. 5. Time series change in number of cars and motorcycles in different functional zones. X axis represents time from 00:00–24:00. N 1, 6 … n represent 1 a.m., 6 am… on weekday. w2, w7 … w_n represent 2 a.m., 6 a.m. on weekend.

emissions.

5. Discussion

The study continuously measured the level of the pollutant emissions in different functional zones during the 24 h of Monday to Sunday. The results indicate that the various urban functional zones have a clear influence on spatial-temporal patterns in terms of the types of vehicle and the total number of vehicles and, thereby, the level of pollutant emissions.

5.1. Pollutant emissions in different functional zones

We observed temporal changes in pollutant emissions on weekdays and at weekends. The samples taken in the residential zones (R3, R5, and R6), industrial zone (I2), and the business zone (B1) revealed clear morning (6:00–9:00) and evening peak periods (17:00–19:00) on weekdays. This is very likely due to job-house commuting, resulting in heavy traffic between the residential zones and areas of employment (industrial zone and business zone) during peak hours (Fig. 5). Site R5 displayed higher PM2.5 and VOC emissions at weekends than on weekdays, which may be because R5 is located next to a suburban area, where motorcycle-taxis are frequently used for the last mile of journey as final destinations are often located far from bus and metro stations. These residential zones developed around pre-existing villages, the residents of which commonly use motorcycles. Many of the motorcycles are relatively old and emit high levels of VOC due to their low initial cost, which have the potential to harm human health in the industrial and residential zones (Fiedler et al., 2005). The emissions at the sites in the business zone were higher at the weekend than on weekdays. The business zone includes retail outlets, entertainment venues, sports facilities and other public services. Citizens visit the area in their leisure time because they cannot access similar facilities that are adjacent to where they live. Consequently, people visit the business zone by car, taxi or motorcycle as the distance is too far to travel by non-motorized transport, i.e. walking and cycling. Therefore, this results in higher emissions at the weekend. The industrial zone exhibited the highest emissions of PM2.5 and PM1.0 of all the areas, which is probably because the area has the highest volume of buses and trucks. In general, the highest level of pollutants was recorded on the expressways, followed by the roads in the business zones on weekdays. Ideally, residents who are sensitive to certain pollutants should avoid rush-hour traffic in the residential and industrial zones and should not live near expressways. Hence, the land adjacent to the expressways should be developed for a different function than residential housing.

This observed relationship between spatio-temporal patterns of traffic-related pollutant emissions and urban functional zones could support urban planning and strategies for reducing pollutant emissions. From the perspective of urban planning, spatio-temporal patterns of traffic-related pollutant emissions represent an important criterion for functional zone planning. The high level of mixed functional zones bring jobs, public services, entertainment venues closer to where people live, thereby reducing journeys and dependency on motorized vehicles, thereby also eventually leading to a decrease in pollutant emissions (Zhao et al., 2018a, 2018b; Zhang et al., 2016). According to temporal changes of traffic-related air pollutants emissions in different zone, practical urban planning were suggested to control specific vehicle types and

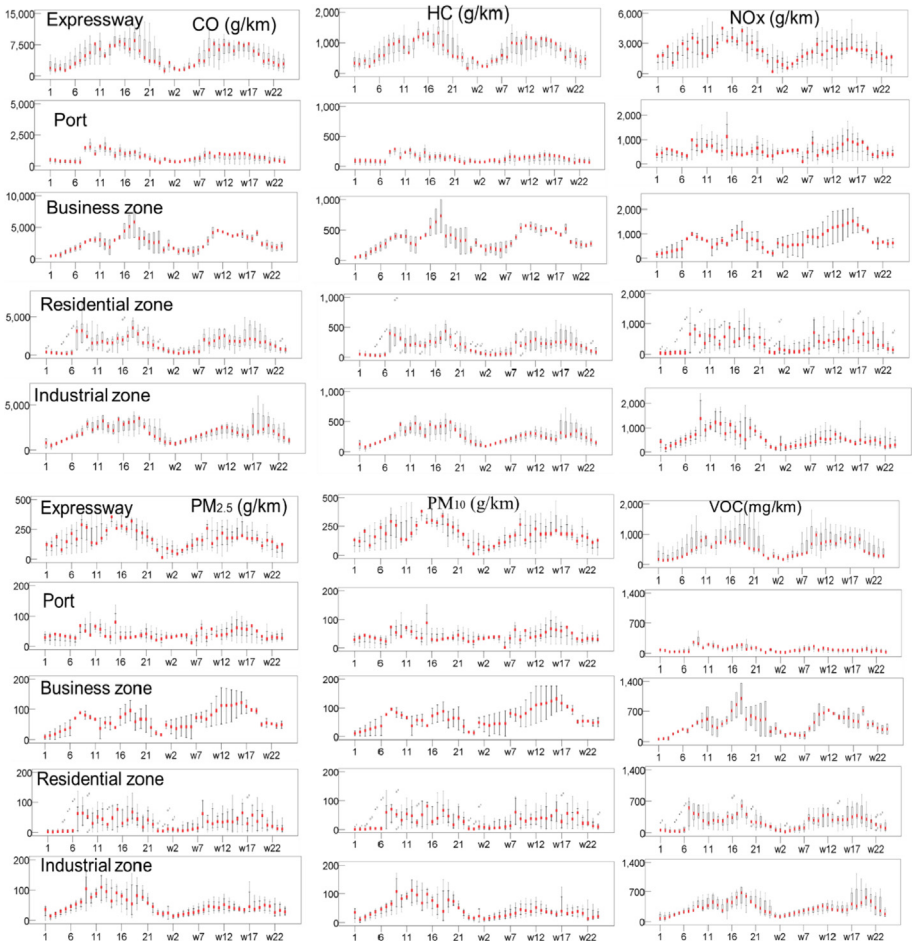

Fig. 6. Time series change in pollutant emissions on weekdays and at weekends in each functional zone.

numbers. For instance, motorcycles should be limited at R6 and I2 during the morning peak (08:00–09:00) as emissions of VOC from motorcycles occupied 57.13% and 53.91%, respectively.

From the perspective of traffic management and climate change, the specification of spatio-temporal patterns of traffic-related pollutant emissions could support the creation of more effective policy instruments for reducing pollutant emissions. For example, the 24/7 traffic management and emission reduction scheme for improving air quality which has been implemented in London, whereby drivers of vehicles that do not meet the Ultra-Low Emission Zone standard have to pay a daily charge to travel within central London. However, this daily and global way of charging is based on coarse spatio-temporal resolution. Instead, a more specific Ultra-Low Emission Zone could be based on the spatio-temporal pattern of traffic-related pollution as such an approach to measuring traffic-related air pollutant emissions is cost-saving with high spatio-temporal resolution. It could potentially be used to map the spatio-temporal pattern of air pollution to accurately control traffic flow in an Ultra-Low Emission Zone instead implementing a daily and global charge.

In terms of air pollution, the detailed spatio-temporal patterns of traffic-related air pollutant emissions could be used to simulate pollution diffusion in different circumstances. This would also help to identify the different sources of the pollution, thereby contributing to the alleviation of air pollution in urban areas. Different driver behaviors may influence the air pollutants emissions, such as speed, mileage and building environment. Previous studies in our study area showed that higher CO emission occurs more frequently under higher speeds (60–75 km/h). The correlation between emission of HC and NOx and speed is relatively week (Huang et al., 2016). Spatial variations of air pollutants in urban building environment (Tong et al., 2019). Future studies are suggested to conduct field measurement by using mobile equipment to examine real vehicle-related air pollution emission and compare the different exposure to in-cabin and out-cabin human health (Tong et al., 2011).

5.2. Advantage of video-based detection

Video-based vehicle detection represents a novel approach to quantifying and analyzing spatio-temporal patterns of traffic-related pollutant emissions. Researchers can benefit from mining spatio-temporal patterns as it can enrich specialized knowledge that crosses the related fields, e.g. urban planning, traffic management and air pollution.

Compared with the traditional way of collecting data, vehicle classification based on deep learning is considered economical, practical and efficient in terms of obtaining traffic-related pollution data, particularly in under-developed suburbs where the number of air quality measurement stations is insufficient due to construction and maintenance costs. In the big data era, real-time video from traffic surveillance cameras could provide high spatio-temporal resolution traffic data that allows the data to be integrated, visualized and analyzed effectively and comprehensively. With the

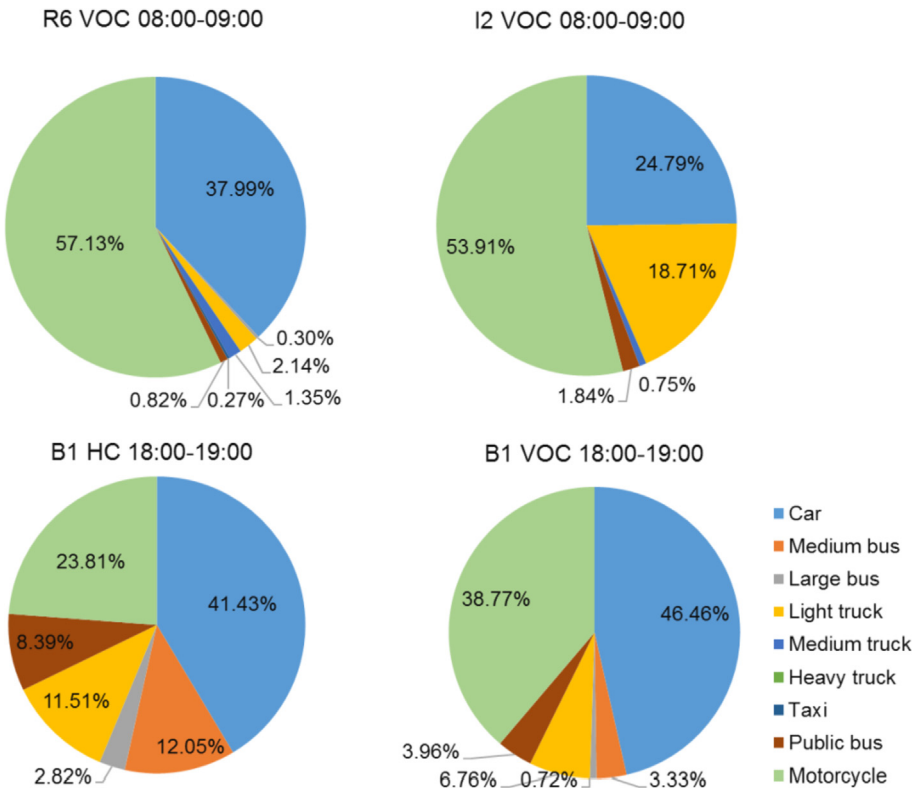

Fig. 7. Air pollutant emissions in the most polluted functional zones on weekdays: R6, VOC 08:00–09:00; I2, VOC 08:00–09:00; B1, HC 18:00–19:00; B1, VOC 18:00–19:00.

development of image recognition, updated YOLO and other real-time detection approaches could improve the accuracy of air pollution estimation. Laboratory chassis dynamometer tests found that vehicle speed has various effects on pollution level according to vehicle type (Lozhkina, 2016; Mamakos et al., 2004; Ntziachristos, 2000; Alves et al., 2015; Zachariadis et al., 2001; Zielinska et al., 2012). Labeles of vehicle form and speed could be used to determine the production date of vehicles, thereby facilitating the calculation of pollutant emissions.

Traffic-related air pollutants, which are considered a major source of air pollution, represent one type of air pollutant in terms of moving source data (Goyal et al., 2006). Air pollutants originate from different anthropogenic processes, which can be categorized into the following source groups: motor traffic, industry, power plants, trade and domestic fuel. Future studies could use the results of this study to develop a more accurate and realistic three-dimensional air pollution simulation which takes as many of the relevant factors, e.g. wind direction, weather, surrounding built environment into consideration as possible.

6. Conclusion

This study has explored the relationship between spatial-temporal patterns of traffic-related air pollutant emissions in different urban functional zones. Vehicles on the expressways and urban roads in the different functional zones were detected and counted by real-time traffic surveillance cameras and a deep learning technique. The pollutant emissions were calculated based on vehicle numbers and pollutant emissions coefficients. The results showed that traffic-related pollutant emissions varied across different functional zone. Except for expressway, the business zones had the highest pollutants emissions. Cars and motorcycles contributed the major traffic-related pollutant emissions to urban environment.

This provided real-time air pollutant emissions data with high spatio-temporal resolution that supports policy-making in different sectors, e.g. urban planning and air pollution control. The study contributes to the literature by introducing a novel cost-saving data collection method: video-based vehicle detection that improves the spatio-temporal resolution of traffic-related air pollution, and reveals the relationship between this pattern and functional zones in more detail, which improves knowledge for controlling traffic-related air pollution. The method has great potential for application in similar studies in other cities.

Acknowledgments

The China Scholarship Council Foundation provided support for this research. We would also like thank Fabian Cristian Gieseke, Assistant Professor from the Department of Computer Science, the University of Copenhagen for sharing his knowledge on image recognition and deep learning.

References

Al-smadi, M., 2016. Traffic Surveillance : a review of vision based vehicle detection. Recognition and Tracking 11, 713–726.

Brauer, M., Hoek, G., Van Vliet, P., Meliefste, K., Fischer, P.H., Wijga, A., Koopman, L.P., Neijens, H.J., Gerritsen, J., Kerkhof, M., Heinrich, J., Bellander, T., Brunekreef, B., 2002. Air pollution from traffic and the development of respiratory infections and asthmatic and allergic symptoms in children. Am. J. Respir. Crit. Care Med. 166, 1092–1098. https://doi.org/10.1164/rccm.200108-007OC.

Brugge, D., Durant, J.L., Rioux, C., 2007. Near-highway pollutants in motor vehicle exhaust: a review of epidemiologic evidence of cardiac and pulmonary health risks. Environ. Health Glob. Access Sci. Source 6, 1–12. https://doi.org/10.1186/1476-069X-6-23.

Buzzelli, M., Jerrett, M., Buzzelli, M., Jerrett, M., 2011. Global Environmental Change Part B : Environmental Hazards Comparing Proximity Measures of Exposure to Geostatistical Estimates in Environmental Justice Research Comparing Proximity Measures of Exposure to Geostatistical Estimates in Environmental Justice

Research 2867. https://doi.org/10.1016/j.hazards.2003.11.001.
Cao, X., Jason, 2017. Land use and transportation in China. Transp. Res. Part Transp. Environ. 52 (Part B), 423–427. Land use and transportation in China. https://doi.org/10.1016/j.trd.2017.02.007.
Clougherty, J.E., Wright, R.J., Baxter, L.K., Levy, J.I., 2008. Land use regression modeling of intra-urban residential variability in multiple traffic-related air pollutants. Environ. Health Glob. Access Sci. Source 7, 1–14. https://doi.org/10.1186/1476-069X-7-17.
Colvile, R.N., Hutchinson, E.J., Mindell, J.S., Warren, R.F., 2001. The Transport Sector as a Source of Air Pollution, vol. 35.
Dons, E., Poppel, M. Van, Kochan, B., Wets, G., Int, L., 2013a. Modeling temporal and spatial variability of traf fi c-related air pollution : hourly land use regression models for black carbon. Atmos. Environ. 74, 237–246. https://doi.org/10.1016/j.atmosenv.2013.03.050.
Dons, E., Temmerman, P., Van Poppel, M., Bellemans, T., Wets, G., Int Panis, L., 2013b. Street characteristics and traffic factors determining road users' exposure to black carbon. Sci. Total Environ. 447, 72–79. https://doi.org/10.1016/j.scitotenv.2012.12.076.
Duvall, R.M., Norris, G.A., Burke, J.M., Olson, D.A., Vedantham, R., Williams, R., 2012. Determining spatial variability in PM2.5 source impacts across Detroit, MI. Atmos. Environ. 47, 491–498. https://doi.org/10.1016/j.atmosenv.2011.09.071.
Esteva, A., Kuprel, B., Novoa, R.A., Ko, J., Swetter, S.M., Blau, H.M., Thrun, S., 2017. With Deep Neural Networks. Nat. Publ. Group. https://doi.org/10.1038/nature21056.
Ewing, R., Cervero, R., 2010. Travel and the built environment. J. Am. Plan. Assoc. 76, 265–294. https://doi.org/10.1080/01944361003766766.
Fiedler, N., Laumbach, R., Kelly-mcneil, K., Lioy, P., Fan, Z., Zhang, J., Ottenweller, J., Ohman-strickland, P., Kipen, H., 2005. Health Effects of a Mixture of Indoor Air Volatile Organics. Their Ozone Oxidation Products , and Stress, pp. 1542–1548. https://doi.org/10.1289/ehp.8132.
Goyal, S.K., Ghatge, S.V., Nema, P., M. Tamhane, S., 2006. Understanding urban vehicular pollution problem vis-a-vis ambient air quality – case study of a megacity (Delhi, India). Environ. Monit. Assess. 119 (1), 557–569. https://doi.org/10.1007/s10661-005-9043-2.
Girshick, Ross, 2015. In: The IEEE International Conference on Computer Vision. ICCV, pp. 1440–1448.
Gordian, M.E., Haneuse, S., Wakefield, J., 2006. An investigation of the association between traffic exposure and the diagnosis of asthma in children. J. Expo. Sci. Environ. Epidemiol. 16, 49–55. https://doi.org/10.1038/sj.jea.7500436.
Hassani, A., Hosseini, V., 2016. An assessment of gasoline motorcycle emissions performance and understanding their contribution to Tehran air pollution. Transportation Research Part D: Transport and Environment 47, 1–12.
Henderson, S.B., 2007. Application of land use regression to estimate long-term concentrations of traffic-related nitrogen oxides and. Fine Particulate Matter 41, 2422–2428. https://doi.org/10.1021/es0606780.
Hochadel, M., Heinrich, J., Gehring, U., Morgenstern, V., Kuhlbusch, T., Link, E., Wichmann, H.E., Krämer, U., 2006. Predicting long-term average concentrations of traffic-related air pollutants using GIS-based information. Atmos. Environ. 40, 542–553. https://doi.org/10.1016/j.atmosenv.2005.09.067.
Hoek, G., Brunekreef, B., Verhoeff, A., Wijnen, J. Van, Hoek, G., Brunekreef, B., Fischer, P., 2011. Daily Mortality and Air Pollution in the Netherlands TECHNICAL Daily Mortality and Air Pollution in the Netherlands, vol. 2247. https://doi.org/10.1080/10473289.2000.10464182.
Hoogh, K. De, Chen, J., Gulliver, J., Ho, B., Hertel, O., Ketzel, M., Bauwelinck, M., Donkelaar, A. Van, Hvidtfeldt, U.A., Katsouyanni, K., Klompmaker, J., Martin, R.V., Samoli, E., Schwartz, P.E., Stafoggia, M., Bellander, T., Strak, M., Wolf, K., Vienneau, D., Brunekreef, B., Hoek, G., 2018. Spatial PM 2 . 5 , NO 2 , O 3 and BC models for western Europe –. Evaluation of spatiotemporal stability 120, 81–92. https://doi.org/10.1016/j.envint.2018.07.036.
Huang, X., Wang, Y., Xing, Z., Du, K., 2016. Emission factors of air pollutants from CNG-gasoline bi-fuel vehicles: Part II. CO, HC and NOx. Sci. Total Environ. 565, 698–705.
Jerrett, M., 2009. Global Geographies of Injustice in Traffic-Related Air Pollution Exposure, 20. https://doi.org/10.1097/EDE.0b013e31819776a1, 2002–2004.
Jerrett, M., Arain, A., Kanaroglou, P., Beckerman, B., Potoglou, D., Sahsuvaroglu, T., Morrison, J., Giovis, C., 2005. A review and evaluation of intraurban air pollution exposure models. J. Expo. Anal. Environ. Epidemiol. 15, 185–204. https://doi.org/10.1038/sj.jea.7500388.
Kampa, M., Castanas, E., 2008. Human health effects of air pollution 151, 362–367. https://doi.org/10.1016/j.envpol.2007.06.012.
Karner, A.A., Eisinger, D.S., Niemeier, D.A., 2010. Near-roadway air quality: Synthesizing the findings from real-world data. Environ. Sci. Technol. 44, 5334–5344. https://doi.org/10.1021/es100008x.
Kim, K., Kabir, E., Kabir, S., 2015. A review on the human health impact of airborne particulate matter. Environ. Int. 74, 136–143. https://doi.org/10.1016/j.envint.2014.10.005.
Kimbrough, S., Baldauf, R.W., Hagler, G.S.W., Shores, R.C., Mitchell, W., Whitaker, D.A., Croghan, C.W., Vallero, D.A., 2013. Long-term continuous measurement of near-road air pollution in Las Vegas: seasonal variability in traffic emissions impact on local air quality. Air Qual. Atmosphere Health 6, 295–305. https://doi.org/10.1007/s11869-012-0171-x.
Kockelman, K., 1997. Travel behavior as function of accessibility, land use mixing, and land use balance: evidence from San Francisco Bay Area. Transp. Res. Rec. J. Transp. Res. Board 116–125.
Künzli, N., Kaiser, R., Medina, S., Studnicka, M., Chanel, O., Filliger, P., Herry, M., Horak, F., Puybonnieux-Texier, V., Quénel, P., Schneider, J., Seethaler, R., Vergnaud, J.C., Sommer, H., 2000. Public-health impact of outdoor and traffic-related air pollution: a European assessment. Lancet 356, 795–801. https://doi.org/10.1016/S0140-6736(00)02653-2.
Leibe, B., Hutchison, D., 2016. Computer Vision – ECCV 2016.
Lelieveld, J., Evans, J.S., Fnais, M., Giannadaki, D., Pozzer, A., 2015. The contribution of outdoor air pollution sources to premature mortality on a global scale. https://doi.org/10.1038/nature15371.
Levy, I., Levin, N., Schwartz, J.D., Kark, J.D., 2015. Back-Extrapolating a Land Use Regression Model for Estimating Past Exposures to Tra Ffi C-Related Air Pollution. https://doi.org/10.1021/es505707e.
Lozhkina, O.V., Lozhkin, V.N., 2016. Estimation of nitrogen oxides emissions from petrol and diesel passenger cars by means of on-board monitoring : Effect of vehicle speed , vehicle technology , engine type on emission rates. Transp. Res. 47 (Part D), 251–264. https://doi.org/10.1016/j.trd.2016.06.008.
Mamakos, A., Ntziachristos, L., Samaras, Z., 2004. Measurements between Vehicle Testing Laboratories : a Long Way to Go. https://doi.org/10.1088/0957-0233/15/9/024.
NA, Kwangsam, et al., 2015. Impact of biodiesel and renewable diesel on emissions of regulated pollutants and greenhouse gases on a 2000 heavy duty diesel truck. Atmospheric Environment 107, 307–314.
Ntziachristos, L., Samaras, Z., 2000. Speed-dependent Representative Emission Factors for Catalyst Passenger Cars and in # Uencing Parameters 34.
Redmon, J., Divvala, S., Girshick, R., Farhadi, A., 2016. In: The IEEE Conference on Computer Vision and Pattern Recognition. CVPR, pp. 779–788 (You Only Look Once : Unified , Real-Time Object Detection).
Riediker, M., Cascio, W.E., Griggs, T.R., Herbst, M.C., Bromberg, P.A., Neas, L., Williams, R.W., Devlin, R.B., 2001. Particulate Matter Exposure in Cars Is Associated with Cardiovascular Effects in Healthy Young Men. https://doi.org/10.1164/rccm.200310-1463OC.
Roemer, W.H., Wijnen, J.H. Van, Roemer, W.H., Wijnen, H. Van, 2018. Linked References Are Available on JSTOR for This Article : Daily Mortality and Air Pollution along Busy Streets in Amsterdam, vol. 12, pp. 649–653, 1987-1998.
Rosenlund, M., Forastiere, F., Stafoggia, M., Porta, D., Perucci, M., Ranzi, A., Nussio, F., Perucci, C.A., 2008. Comparison of Regression Models with Land-Use and Emissions Data to Predict the Spatial Distribution of Traffic-Related Air Pollution in Rome, pp. 192–199. https://doi.org/10.1038/sj.jes.7500571.
Alves, Célia A, et al., 2015. Elements and Polycyclic Aromatic Hydrocarbons in Exhaust Particles Emitted by Light-Duty Vehicles. Environmental Science and Pollution Research 22 (15), 11526–11542.
Shekarrizfard, M., Faghih-imani, A., Crouse, D.L., Goldberg, M., Ross, N., Eluru, N., Hatzopoulou, M., 2016. Individual exposure to traffic related air pollution across land-use clusters. Transp. Res. Part D 46, 339–350. https://doi.org/10.1016/j.trd.2016.04.010.
Song, J., Lin, T., Li, X., Prishchepov, V.A., 2018. Mapping urban functional zones by integrating very high spatial resolution remote sensing imagery and points of interest: a case study of Xiamen, China. Remote Sens. 10 (11), 1737. https://doi.org/10.3390/rs10111737.
Song, J., Zhao, C., Zhong, S., Nielsen, T.A.S., Prishchepov, A.V., 2019a. Mapping spatio-temporal patterns and detecting the factors of traffic congestion with multi-source data fusion and mining techniques. Comput. Environ. Urban Syst. 77, 101364.
Song, J., Tong, X., Wang, L., Zhao, C., Prishchepov, A.V., 2019b. Monitoring finer-scale population density in urban functional zones: a remote sensing data fusion approach. Landsc. Urban Plan. 103580.
Tong, Z., Wang, Y.J., Patel, M., Kinney, P., Chrillrud, S., Zhang, K.M., 2011. Modeling spatial variations of black carbon particles in an urban highway-building environment. Environ. Sci. Technol. 46 (1), 312–319.
Tong, Z., Li, Y., Westerdahl, D., Adamkiewicz, G., Spengler, J.D., 2019. Exploring the effects of ventilation practices in mitigating in-vehicle exposure to traffic-related air pollutants in China. Environ. Int. 127, 773–784.
Vardoulakis, S., Fisher, B.E.A., Pericleous, K., Gonzalez-flesca, N., 2003. Modelling air quality in street canyons : Review 37, 155–182.
Wang, R., Henderson, S.B., Sbihi, H., Allen, R.W., Brauer, M., 2013. Temporal stability of land use regression models for traf fi c-related air pollution. Atmos. Environ. 64, 312–319. https://doi.org/10.1016/j.atmosenv.2012.09.056.
Wu, C., Zeng, Y., Lung, S.C., 2018. Science of the Total Environment A hybrid kriging/land-use regression model to assess PM 2 . 5 spatial-temporal variability. Sci. Total Environ. 645, 1456–1464. https://doi.org/10.1016/j.scitotenv.2018.07.073.
Xu, D., Yan, Y., Ricci, E., Sebe, N., 2017. Detecting anomalous events in videos by learning deep representations of appearance and motion. Comput. Vis. Image Understand. 156, 117–127. https://doi.org/10.1016/j.cviu.2016.10.010.
XMHOUSE, 2016. http://news.xmhouse.com/bd/201612/t20161215_631809.htm.
Yang, W., Yu, C., Yuan, W., Wu, X., Zhang, W., Wang, X., 2018. High-resolution vehicle emission inventory and emission control policy scenario analysis , a case in the Beijing-Tianjin-Hebei (BTH) region , China. J. Clean. Prod. 203, 530–539. https://doi.org/10.1016/j.jclepro.2018.08.256.
Zachariadis, T., Ntziachristos, L., Samaras, Z., 2001. The e ∈ ect of age and technological change on motor vehicle emissions, vol. 6, pp. 221–227.
Zhang, Y., Li, C., Ding, C., Zhao, C., Huang, J., 2016. The built environment and the frequency of cycling Trips by urban elderly:
Insights from Zhongshan, China. J. Asian Architect. Build Eng. 15, 511–518. https://doi.org/10.3130/jaabe.15.511.
Zhao, C., Nielsen, T.A.S., Olafsson, A.S., Carstensen, T.A., Fertner, C., 2018a. Cycling environmental perception in Beijing – a study of residents' attitudes towards

future cycling and car purchasing. Transp. Policy 66, 96–106. https://doi.org/10.1016/j.tranpol.2018.02.004.

Zhao, C., Nielsen, T.A.S., Olafsson, A.S., Carstensen, T.A., Meng, X., 2018b. Urban form, demographic and socio-economic correlates of walking, cycling, and e-biking: evidence from eight neighborhoods in Beijing. Transp. Policy 64, 102–112. https://doi.org/10.1016/j.tranpol.2018.01.018.

Zhou, Y., Cheng, S., Lang, J., Chen, D., Zhao, B., 2015. A comprehensive ammonia emission inventory with high-resolution and its evaluation in the Beijing e Tianjin e Hebei (BTH) region , China. Atmos. Environ. 106, 305–317. https://doi.org/10.1016/j.atmosenv.2015.01.069.

Zielinska, B., Sagebiel, J., Mcdonald, J.D., Whitney, K., Lawson, D.R., Zielinska, B., Sagebiel, J., Mcdonald, J.D., Whitney, K., Zielinska, B., Sagebiel, J., Mcdonald, J.D., Lawson, D.R., 2012. Emission Rates and Comparative Chemical Composition from Selected In-Use Diesel and Gasoline-Fueled Vehicles Emission Rates and Comparative Chemical Composition from Selected In-Use Diesel and Gasoline-Fueled Vehicles 2247. https://doi.org/10.1080/10473289.2004.10470973.